Supporting Information

Mercury Isotopes in Deep-sea Epibenthic Biota Suggest Limited Hg Transfer from Photosynthetic to Chemosynthetic Food Webs

Jingjing Yuan[1], Yi Liu[1], Shun Chen[2], Xiaotong Peng[2], Yu-Feng Li[3], Songjing Li[1], Rui Zhang[1], Wang Zheng[1], Jiubin Chen[1], Ruoyu Sun[1], Lars-Eric Heimbürger-Boavida[4]*

[1]Institute of Surface-Earth System Science, School of Earth System Science, Tianjin University, 300072 Tianjin, China.

[2]Deep Sea Science Division, Institute of Deep Sea Science and Engineering, Chinese Academy of Sciences, 572000 Sanya, Hainan, China.

[3]CAS-HKU Joint Laboratory of Metallomics on Health and Environment, CAS Key Laboratory for Biomedical Effects of Nanomaterials and Nanosafety, Beijing Metallomics Facility, Institute of High Energy Physics, Chinese Academy of Sciences, 100049 Beijing, China.

[4]Aix Marseille Université, CNRS/INSU, Université de Toulon, IRD, Mediterranean Institute of Oceanography (MIO) UM 110, 13288 Marseille, France.

Corresponding Author

*Ruoyu Sun (ruoyu.sun@tju.edu.cn).

Pages: 18

Text: S1-S3 (Page S3-S6)

Figures: S1-S4 (Page S7-S10)

Tables: S1-S3 (Page S11-S16)

References: Page S17-S18

Text S1 Study Area

The Indian Ocean has three spreading ridge branches, the Central Indian Ridge (CIR), the Southwest Indian Ridge (SWIR), and the Southeast Indian Ridge (SEIR). Their spreading rates vary from the ultraslow for the SWIR (7 to 16 mm yr^{-1}) to the intermediate for the SEIR and CIR (50 to 60 mm yr^{-1}). The Indian Ocean Ridge is a major tectonic province that provides the migration route for the chemosynthetic deep-sea vent fauna between the Atlantic and Pacific Oceans [1]. At all selected vent fields, endo- and epi-symbioses between bacteria and biota are responsible for sustaining the high biomass of vent communities [2]. The selected Longqi (37°56'S, 49°39'E; ~2755 m water depth) and Duanqiao hydrothermal fields (HFs, 37°39'S, 50°24'E; ~1739 m water depth) are situated between the hydrothermal-activate Indomed and Gallieni Fracture Zones of the SWIR system [3-5]. Longqi HF consists of sulfide chimneys and massive sulfides with an assemblage of relatively low-temperature mineral associations including abundant amorphous silica and sphalerite [3]. Sulfides in the Duanqiao HF mainly consist of high-temperature minerals such as chalcopyrite and pyrite [5]. The Kairei HF (25°19'S, 70°02'E; ~2450 m water depth) and the Edmond HF (23°53'S, 69°36'E; ~3300 m water depth) are located at the southern portion of the CIR from 23°S to the Rodriguez Triple Junction near 25°30'S [6, 7]. Near the Kairei HF, patchy olivine-rich intrusions are scattered within mantle ultramafic rocks, revealing that infiltrated seawater used to react with magma and ultramafic rocks or olivine-rich rocks. The deeper Edmond HF is located at ~160 km north of the Kairei HF. Hydrothermal vents at Edmond exhibit a wide range of styles and chimney morphologies, and the extensive diffuse flows and blocks of anhydrite suggest that sub-surface seawater entrainment and mixing processes occur over a broad area [6].

Cold seeps are formed as a result of tectonic fluid expulsion by the dewatering of sediments in response to lateral compression by plate movement. The cold seeps from the South China Sea occur on the

northwestern continental slope and are characterized by patches of authigenic carbonate rocks protruding from the muddy seafloor [8, 9]. At least two seepage sites have been identified, in which the Site F (also called Formosa Ridge; 22.12°N, 119.29°E) cold seep is at a water depth of 1120 m. The study of the communities from cold seeps on both sides of the Atlantic (Gulf of Mexico, Barbados, and Gulf Guinea) revealed that two distant seepage sites can share several important species and possess very closely related communities [1].

Text S2 THg and MMHg Concentration Analysis and QA/QC

The total mercury (THg) concentrations were quantified by cold vapor atomic absorption spectrometry (CV-AAS, DMA-80 evo Direct Mercury Analyzer) following the US-EPA method 7473 [10]. In detail, approximately 0.05-0.1 g of each sample was weighed into a nickel boat, and fully covered with Hg-free diatomite to avoid sample losses during heating and blowing before sending the boat to the auto-sampler for following thermal decomposition. The thermally released Hg vapor was amalgamated with gold, and then desorbed and detected by an atomic absorption spectroscopy (AAS). The quality assurance (QA) and quality control (QC) were conducted using method/sample blanks, sample replicates, and certified reference materials (CRMs, DORM-4, dogfish muscle; NIST SRM-2702, marine sediment). Method blanks were <1% of the Hg mass of the measured samples. The average recoveries were 98 ± 4% as assessed by DORM-4 and 102 ± 9% by NIST SRM-2702. The relative standard deviations of sample/CRM duplicates were <5% for THg concentrations.

Monomethylmercury (MMHg) concentrations in biota were measured by a cold vapor gas chromatography atomic fluorescence spectrometry (CV-GC-AFS, Tekran 2700) according to the US-EPA method 1630 [11]. In detail, approximately 0.01-0.06 g of each sample was weighed into an 8 mL brown glass bottle where 4 mL of 25% (m/v) KOH/CH_3OH solution was added. The mixture was shaken for 4 h at 37 °C with a speed of 240 rpm. After cooling down to room temperature, each digested solution was diluted with

CH_3OH to an appropriate volume. MMHg concentrations were measured by AFS following a series of steps including aqueous ethylation, purging and trapping, heating desorption, separation by gas chromatography, and thermally reduction to Hg^0. Method blanks were 0.001 ± 0.010 ng g^{-1}. The average recoveries were 106 ± 11% as assessed by CRMs (DORM-4; TORT-3, lobster Hepatopancreas). The relative standard deviations of sample/CRM duplicates were <5% for MMHg concentrations.

Text S3 Stable Hg Isotope Analysis and QA/QC

THg in sulfide and biota was extracted for isotope ratio analysis using acid digestion methods. Aliquots of ~0.02-0.5 g of homogenized sulfide samples were digested using 6 ml bi-distilled HNO_3 and 3 ml bi-distilled HCl in 20 mL Teflon beakers at ~100 °C for 48 hours. Similarly, aliquots of ~0.03-0.7 g of biota samples were digested using 4 ml bi-distilled HNO_3 and 4 ml trace metal grade H_2O_2. After cooling down to ambient temperature, ~0.5 ml of 0.2 M BrCl was then added into the digested solutions to ensure a full conversion of all forms of Hg to inorganic Hg(II). The digested sample solutions were filtered through precleaned glass fiber filters and purified using the anion-exchange chromatographic method to remove organic and elemental matrix that may interfere with isotope measurements [12, 13]. Briefly, each filtered solution was loaded onto a column containing anion exchange resin AG1-X4 (200-400 mesh, Bio-Rad) that was already cleaned and conditioned. After rinsing with 2 M HCl to remove the matrix, Hg was finally eluted with 12 ml of 0.5 M HNO_3 and 0.05% (m/v) L-cysteine. The eluted solution was digested with 0.2 M BrCl before isotope analysis. THg concentrations in the purified sample solutions were measured by a Tekran 2600 cold vapor atomic fluorescence spectrometer (CV-AFS) according to the US-EPA method 1631E [14]. Procedural blanks and CRMs (DORM-4 and TORT-3 for biota; MESS-4, NIST SRM-2702, and NIST SRM-1944 for sulfides) were processed with the samples in the same manner. The procedural blanks accounted for <1% of Hg mass in the samples. The Hg recoveries calculated by comparing the recovered Hg

mass (THg concentrations by Tekran 2600 × volume of purified sample solutions) with Hg mass before digestion (THg concentrations by DMA-80 evo × sample weight) were in the range of 93-103% for the procedural CRMs and 84-108% for the samples. The purified sample solutions were diluted with ultrapure water to Hg concentrations of 0.5-1 ng g^{-1} and were measured for Hg isotope ratios by coupling a customized cold vapor generation system to multi-collector inductively coupled plasma mass spectrometry (MC-ICPMS, Nu Plasma 3D at Tianjin University, China). The typical sensitivity for ^{202}Hg was ~2 V per ng g^{-1} Hg at a solution uptake rate of 0.6 mL min^{-1}. Instrumental mass bias was corrected by both an internal NIST SRM-997 Tl standard solution (supplied via the Aridus II desolvation nebulizer system) using the exponential fractionation law and NIST SRM-3133 Hg standard-sample bracketing method. The bracketed NIST SRM-3133 solutions were matched to the sample solutions within 5% in both acid matrix and Hg concentrations. The Faraday cups were positioned to simultaneously collect six Hg isotopes (^{198}Hg, ^{199}Hg, ^{200}Hg, ^{201}Hg, ^{202}Hg, ^{204}Hg) and two Tl isotopes (^{203}Tl and ^{205}Tl). Acquisition time was 7 min (3 blocks, 33 cycles, 4.2 s of integration time) with 3 min of initial uptake time. Between samples, the system was washed with the sample matrix solution for 10 min to ensure that the blank signals were <1% of the preceding sample or standard signals. The typical internal precisions of Hg isotope ratios (e.g., ^{202}Hg/^{198}Hg) were ≤ 0.04‰ (1SE) for individual analysis. The means and uncertainties of Hg isotope ratios of NIST SRM-8610, TORT-3, DORM-4, MESS-4, NIST SRM-2702, and NIST SRM-1944 were listed in Table S3, which were consistent with the previously reported values [15-19].

Supporting Figures

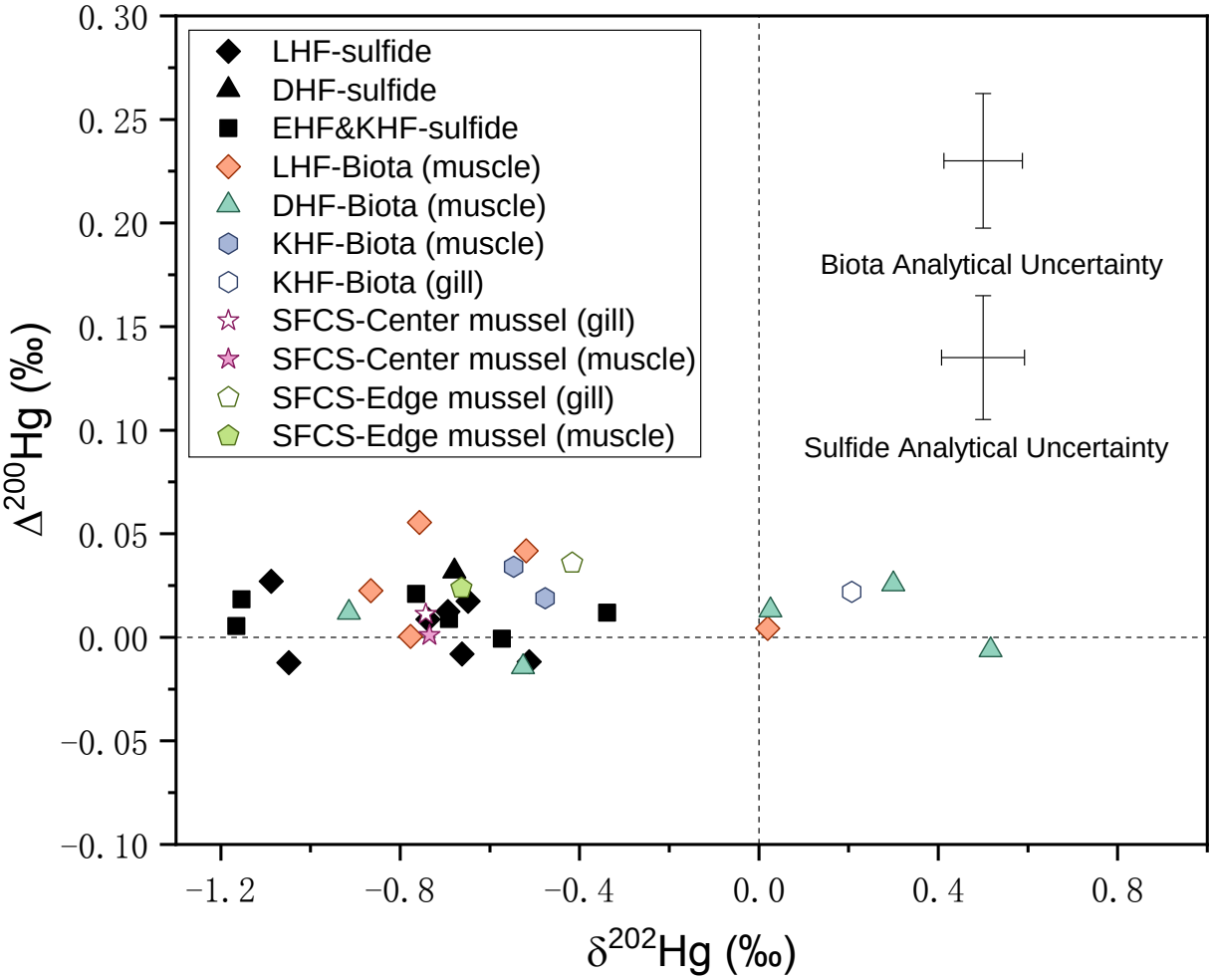

Figure S1. Δ^{200}Hg versus δ^{202}Hg in all hydrothermal biota and sulfides from the Longqi (LHF), Duanqiao (DHF), Endmond (EHF), and Kairei (KHF) hydrothermal fields at the Indian Ocean Ridge, and the Site F cold seep mussels at the South China Sea. Note: SFCS-Center mussel: mussel near the center of the Site F cold seep; SFCS-Edge mussel: mussel at the edge of the Site F cold seep.

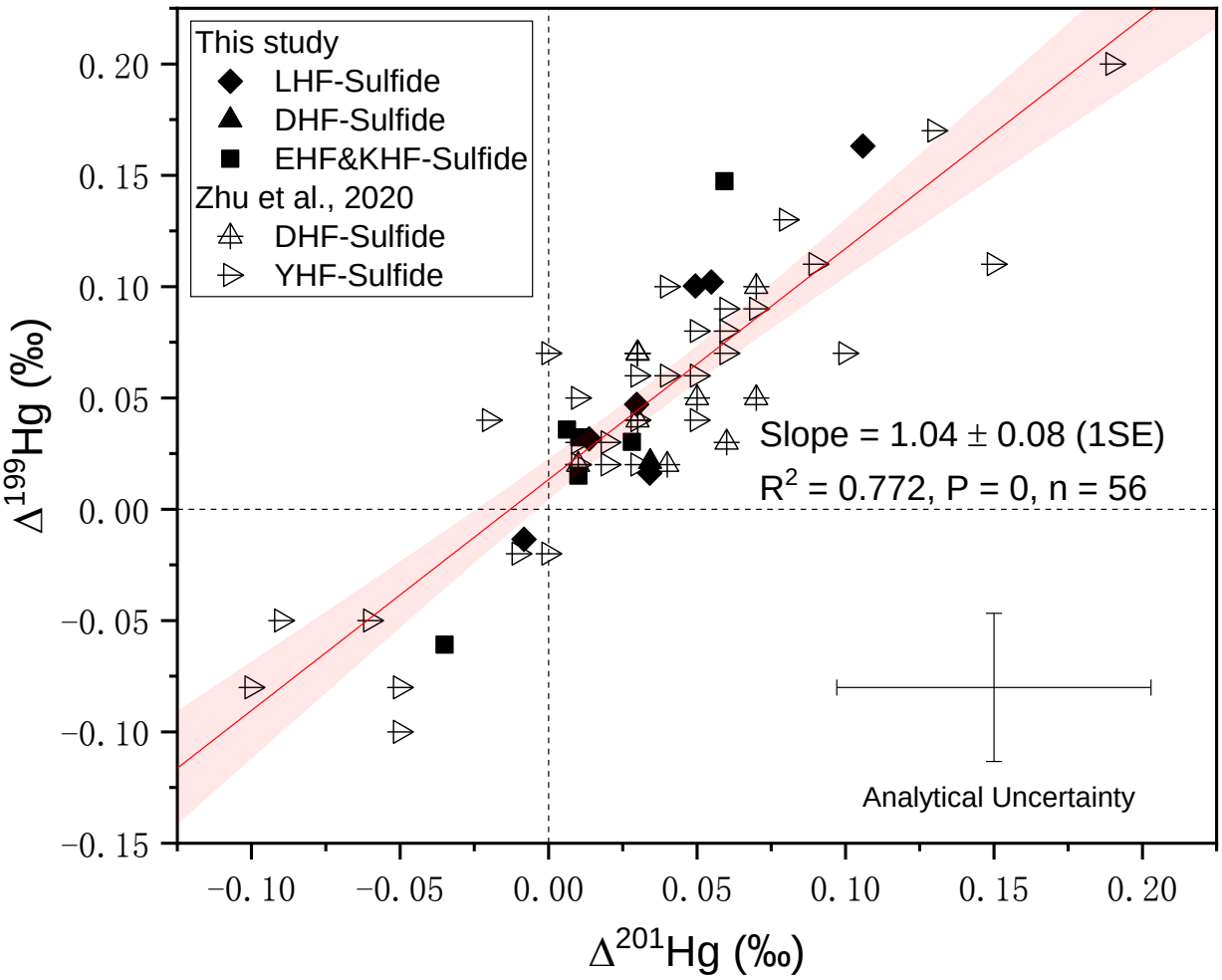

Figure S2. Δ^{199}Hg versus Δ^{201}Hg in all reported hydrothermal sulfides from the Longqi (LHF), Duanqiao (DHF), Yuhuang (YHF), Edmond (EHF), and Kairei (KHF) hydrothermal fields at the Indian Ocean ridge, n is the number of samples.

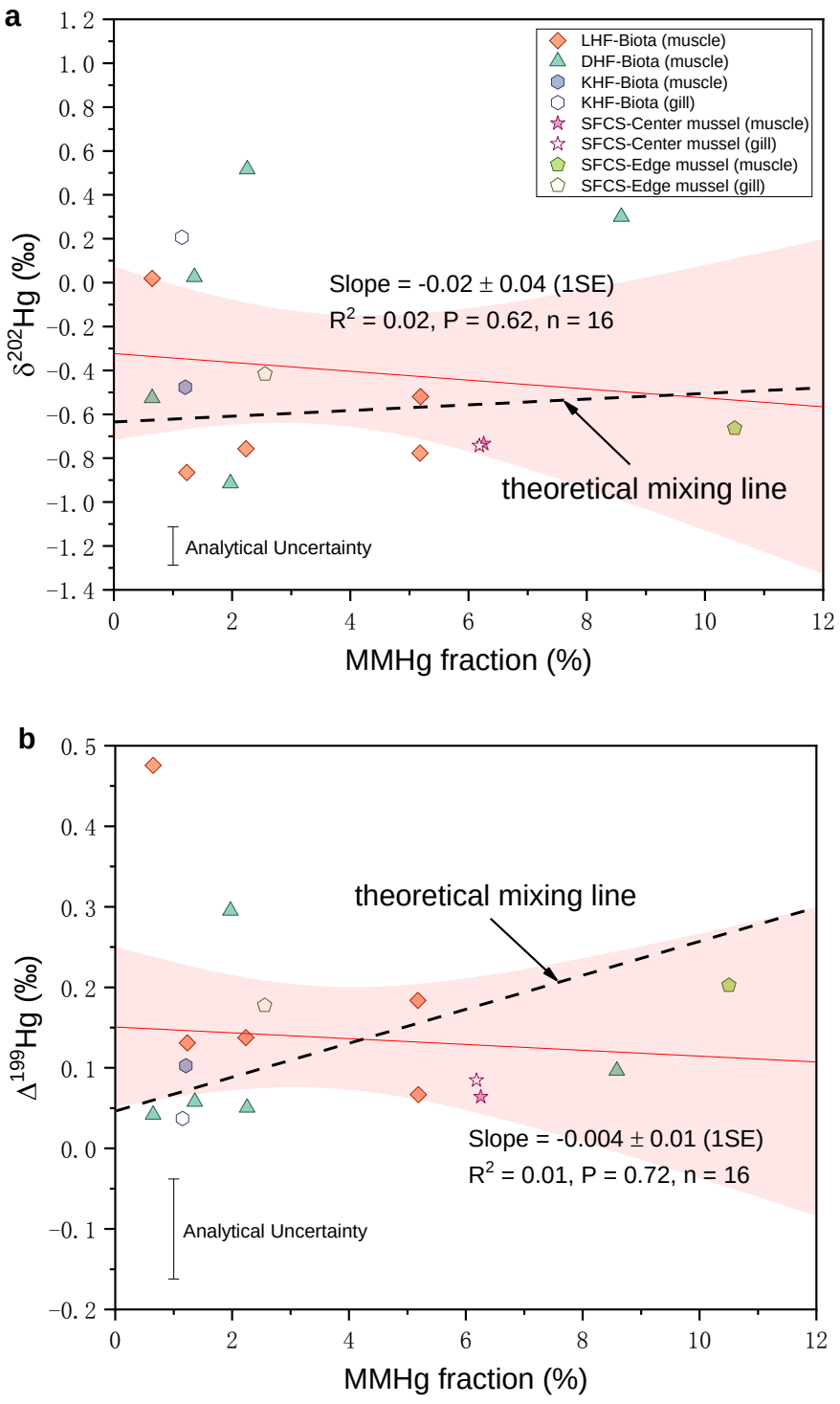

Figure S3. Linear correlations of δ^{202}Hg (a) and Δ^{199}Hg (b) versus MMHg fraction (MMHg%) in all the hydrothermal biota from the Longqi (LHF), Duanqiao (DHF) and Kairei (KHF) hydrothermal fields at the Indian Ocean Ridge and Site F cold seep (SFCS) mussels at the South China Sea. n is the number of samples. Black dashed lines are δ^{202}Hg and Δ^{199}Hg theoretical mixing lines between deep marine inorganic Hg (represented by sulfides, δ^{202}Hg = -0.63‰, Δ^{199}Hg = 0.05‰) and upper marine MMHg (represented by upper ocean marine fishes, δ^{202}Hg = 0.65‰, Δ^{199}Hg = 2.14‰).

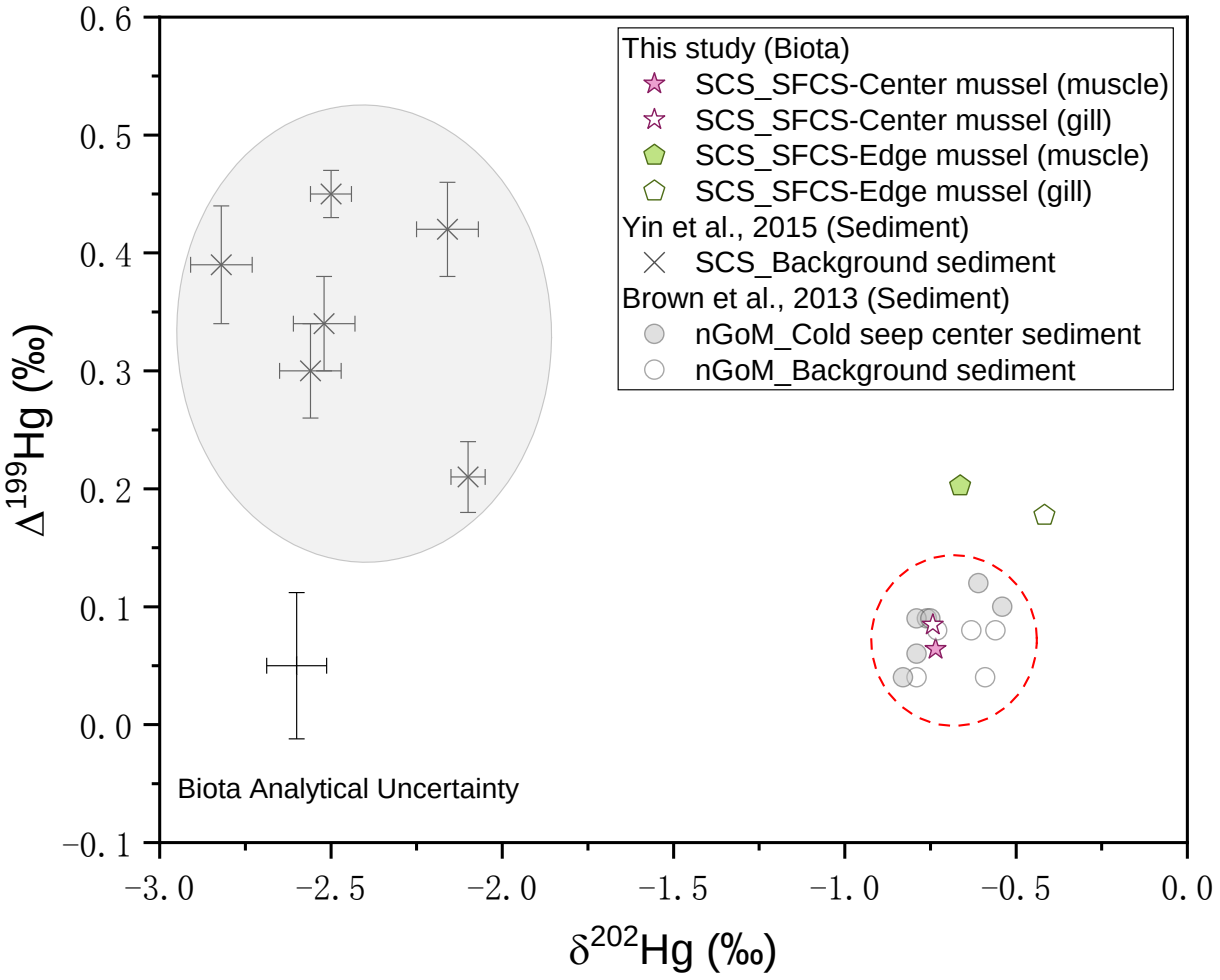

Figure S4. Δ^{199}Hg versus δ^{202}Hg of cold seep mussels and background sediments in the South China Sea (SCS) [20], as well cold seep sediments and background sediments in the northern Gulf of Mexico (nGoM) [21]. Note: SFCS-Center mussel: mussel near the center of the Site F cold seep; SFCS-Edge mussel: mussel at the edge of the Site F cold seep.

Supporting Tables

Supplementary Table 1. THg concentrations and isotope compositions of hydrothermal sulfides and hydrothermally-affected sediments from different hydrothermal fields in Indian Ocean Ridge.

Hydrothermal Vents	Sample ID	Species	Longitude	Latitude	Collection depth (m)	THg (ng g^{-1}, dw)	δ^{202}Hg (‰)	2SD (‰)	Δ^{199}Hg (‰)	2SD (‰)	Δ^{200}Hg (‰)	2SD (‰)	Δ^{201}Hg (‰)	2SD (‰)	Δ^{204}Hg (‰)	2SD (‰)	References
Longqi hydrothermal field (LHF), Southwest Indian Ridge	SY098-G03	Sl-Bs	49.6492°E	37.7827°S	2789	3237	-0.74		0.03		0.01		0.01		-0.03		This study
	SY098-G05	Sl-Bs	49.6487°E	37.7830°S	2789	2842	-1.05		0.05		-0.01		0.03		-0.01		
	SY098-G07	Sl-Bs	49.6492°E	37.7826°S	2789	84.6	-0.72		0.11		0.03		0.07		-0.03		
		Replicate					-0.67		0.09		-0.01		0.03		0.04		
	SY102-G02	Sl-Bs	48.7747°E	37.9629°S	2734	18.6	-0.51		0.16		-0.01		0.11		-0.07		
	SY105-G05	Sl-Bs	49.6497°E	37.7837°S	2782	18217	-1.11		0.10		0.03		0.05		0.05		
		Replicate					-1.07		0.10		0.03		0.06		0.01		
	SY109-G09	Sl-Bs	49.6491°E	37.7827°S	2771	1510	-0.66		-0.01		-0.01		-0.01		0.00		
	SY122-G02	Sl-Bs	49.6479°E	37.7810°S	2783	7.17	-0.65		0.02		0.02		0.03		0.08		
Duanqiao hydrothermal field (DHF), Southwest Indian Ridge	SY114-G02	Sl-Bs	50.4482°E	37.6594°S	1820	147	-0.68		0.02		0.03		0.03		0.03		This study
	34Ⅳ-TVG-08-1-1P	Py				4248	-0.47		0.07				0.03				Zhu, et al.[22]
	34Ⅳ-TVG-08-1-1C	Ccp				346	-0.28		0.02				0.01				
	34Ⅳ-TVG-08-1-2P	Py				6960	-0.63		0.07				0.03				
	34Ⅳ-TVG-08-2-1P	Py				2525	-0.33		0.03				0.06				
	34Ⅳ-TVG-08-2-1P	Py				4268	-0.39		0.05				0.07				
	34Ⅳ-TVG-08-2-2P	Py				2501	-0.12		0.07				0.03				
	34Ⅳ-TVG-08-2-3P	Py				2567	-0.15		0.05				0.05				
	34Ⅳ-TVG-08-4-1P	Py				8121	-0.27		0.02				0.04				
	34Ⅳ-TVG-08-4-2P	Py				5798	-0.25		0.10				0.07				
	34Ⅳ-TVG-08-4-3P	Py				5829	-0.24		0.04				0.03				
	34Ⅱ-TVG-22-1-P	Py				4060	-0.74		0.07				0.06				
	34Ⅱ-TVG-22-2-P	Py				2411	-0.71		0.06				0.05				
	34Ⅱ-TVG-22-3-P	Py				7154	-0.74		0.04				0.05				

Yuhuang hydrothermal field (YHF), Southwest Indian Ridge	34Ⅱ-TVG-22-3-S	Sph				6003	-0.36		-0.02				-0.01				Zhu, et al.[22]
	34Ⅱ-TVG-22-4-P	Py				4924	-0.74		0.09				0.07				
	34Ⅱ-TVG-22-4-S	Sph				3810	-0.10		-0.10				-0.05				
	34Ⅱ-TVG-22-5-P	Py				5292	-0.87		0.07				0.00				
	34Ⅱ-TVG-22-7-P	Py				7314	-0.68		0.10				0.04				
	34Ⅱ-TVG-23-3-S	Sph				2065	-0.65		0.05				0.01				
	34II-TVG-22-2-3	Sph-Md				1905	-0.67		-0.05				-0.06				
	34II-TVG-22-2-4	Sph-Md				1016	-0.05		-0.08				-0.10				
	34II-TVG-23-1-1	Py-Md				10172	-0.94		0.02				0.01				
	34II-TVG-23-1-2	Sph-Md				1410	-0.26		-0.02				0.00				
	34II-TVG-23-1-3	Sph-Md				833	-0.20		-0.08				-0.05				
	34II-TVG-23-1-4	Py-Md				1486	-0.84		0.02				0.02				
	34II-TVG-23-1-5	Py-Md				44035	-0.40		0.06				0.04				
	34II-TVG-23-1-6	Py-Md				2397	-0.50		-0.05				-0.09				
	34II-TVG-23-1-7	Py-Md				1770	-1.07		0.07				0.10				
	34II-TVG-23-1-8	Py-Md				435	-0.85		0.02				0.03				
	34II-TVG-23-1-9	Py-Md				10131	-0.94		0.06				0.03				
	34II-TVG-23-1-10	Py-Md				1104	-0.35		0.04				0.03				
	34II-TVG-23-1-11	Py-Md				2662	-0.53		0.03				0.01				
	34IITVG-22-7-1	Py-Md				9408	-0.64		0.03				0.02				
	34IITVG-22-7-2	Py-Md				7743	-0.94		0.13				0.08				
	34IITVG-22-7-3	Py-Md				2709	-1.23		0.20				0.19				
	34IITVG-22-7-4	Py-Md				2197	-0.90		0.11				0.15				
	34IITVG-22-7-5	Py-Md				956	-0.55		0.04				-0.02				
	34IITVG-22-7-7	Py-Md				1504	-0.48		0.08				0.06				
	34IITVG-22-7-8	Py-Md				5885	-0.87		0.11				0.09				
	34IITVG-22-7-9	Py-Md				1973	-0.90		0.17				0.13				
	34IITVG-22-7-10	Py-Md				11267	-1.03		0.08				0.05				
	34IITVG-22-7-11	Py-Md				3745	-0.87		0.09				0.06				

Edmond & Kairei hydrothermal fields (EHF & KHF), Central Indian Ridge	SY134-G05	Sl-Bs	69.5965°E	23.8784°S	3310	4574	-0.69	0.07	0.03	0.05	0.01	0.09	0.03	0.15	-0.02	0.01	This study
		Replicate					-0.69		0.03		0.00		-0.03		-0.02		
	SY140-G03	Sl-Bs	69.5964°E	23.8780°S	3305	2081	-0.57		0.02		0.00		0.01		0.00		
	SY140-G04	Sl-Bs	69.5964°E	23.8780°S	3305	2570	-0.74	0.21	0.03	0.01	0.03	0.06	0.05	0.03	0.01	0.05	
		Replicate					-0.81		0.03		0.01		-0.02		0.02		
	SY140-G06	Sl-Bs	69.5964°E	23.8780°S	3305	825	-1.17		0.04		0.01		0.01		0.00		
	SY140-G09	Sl-Bs	69.5964°E	23.8780°S	3305	203	-1.15	0.11	0.15	0.03	0.02	0.04	0.06	0.05	0.00	0.02	
	SY142-G02*	Sl-Bs	70.0403°E	25.3205°S	2424	1337	-0.34		-0.06		0.01		-0.03		0.03		
the middle region of Central Indian Ridge	MC1906**	Vp-Ss	66.4237°E	11.4155°S		5329	0.29		-0.14				-0.10				Kim, et al. [23]
	BC1903**	Vp-Ss	66.4238°E	11.4152°S		4435	0.39		-0.14				-0.08				
	MC1912**	Vp-Ss	66.4236°E	11.4150°S		10536	0.06		-0.07				-0.06				
	MC1912***	Vp-Ss	66.4236°E	11.4150°S		12944	-0.20		-0.06				-0.09				
	GTV1907**	Vp-Ss	66.4235°E	11.4162°S		1042	0.26		-0.12				-0.08				
	MC1902**	Vd-Ss	66.4346°E	11.3350°S		376	-1.66		-0.02				0.01				
	MC1803**	Vd-Ss	66.4246°E	11.4150°S		419	-1.29		-0.02				-0.03				
	MC1911**	Vd-Ss	66.4515°E	11.3625°S		129	-1.12		0.11				0.07				
	MC1806**	Vd-Ss	66.4628°E	11.3013°S		146	-0.93		0.09				0.06				
	MC1806***	Vd-Ss	66.4628°E	11.3013°S		176	-0.35		0.09				0.07				
	MC1808**	Vd-Ss	66.4843°E	11.2377°S		139	-1.02		0.03				-0.03				
	GTV1908**	Vd-Ss	68.1382°E	8.1691°S		248	-1.68		0.14				-0.02				
	MC1706**	Vd-Ss	68.1533°E	8.1632°S		53	-1.43		0.12				0.14				
	MC1705**	Vd-Ss	68.1100°E	8.1252°S		140	-0.85		0.20				0.16				
	MC1705***	Vd-Ss	68.1100°E	8.1252°S		126	-0.69		0.13				0.05				
	MC1914**	Vd-Ss	68.1117°E	8.1249°S		105	-1.09		0.11				0.00				

Note: Replicate is for Hg isotopes measurement; dw, dry weight; Sl-Bs, surface layer massive sulfide; Py, handpicked pyrite; Ccp, handpicked chalcopyrite; Sph, handpicked sphalerite; Sph-Md, micro drilling sulfides mainly consist of sphalerite; Py-Md, micro drilling sulfides mainly consist of pyrite; Vp-Ss, Vent-proximal sediment, Vd-Ss, Vent-distal sediment; "*" sulfide from Kairei hydrothermal field at the Central Indian Ridge; "**" surface sediments; "***" subsurface sediments.

Supplementary Table 2. Total Hg and MMHg concentrations, and Hg, carbon, and nitrogen isotope compositions in different body tissues of biota from different hydrothermal fields in Indian Ocean Ridge and the Site F cold seep in the South China Sea.

Sample locations	Sample ID	Species/tissue	Longitude	Latitude	Depth (m)	n	THg (ng g^{-1}, dw)	MMHg (ng g^{-1}, dw)	MMHg/THg (%)	δ^{202}Hg (‰)	2SD (‰)	Δ^{199}Hg (‰)	2SD (‰)	Δ^{200}Hg (‰)	2SD (‰)	Δ^{201}Hg (‰)	2SD (‰)	Δ^{204}Hg (‰)	2SD (‰)	δ^{13}C (‰)	δ^{15}N (‰)
Longqi hydrothermal field (LHF), Southwest Indian Ridge	SY124-shrimp	*Rimicaris exoculate*/ muscle	49.6472°E	37.7792°S	2769	1	11.9	BDL	NA	NA		NA		NA		NA		NA		-13.79	8.69
	SY126-1-mussel	*Bathymodiolus marisindicus*/ muscle	49.6479°E	37.7810°S	2771	4	305	3.8	1.2	-0.87	0.09	0.13	0.01	0.02	0.01	0.09	0.02	0.00	0.06	-36.28	-12.04
	SY126-white snail	*Phymorhynchus sp.*/ muscle	49.6479°E	37.7810°S	2771	1	402	20.8	5.2	-0.78		0.18		0.00		0.13		-0.04		-35.16	-9.81
	SY126-mussel	NA/muscle	49.6479°E	37.7810°S	2771	1	6.0	BDL	NA	NA		NA		NA		NA		NA		-35.28	-7.43
	SY128-gastropod	*Chrysomallon squamiferum*/ muscle	46.6497°E	37.7840°S	2759	3	882	5.7	0.60	0.02		0.47		-0.02		0.32		0.00		NA	NA
	Replicate									0.02		0.48		0.03		0.35		-0.03		NA	NA
	SY128-crab	*Munidopsis sp.*/ muscle	46.6497°E	37.7840°S	2759	NA	114	10.4	5.2	-0.52		0.07		0.04		0.07		-0.02		-16.27	7.91
	SY130-barnacles	*Neolepas sp.*/muscle	49.6490°E	37.7835°S	2775	2	108	2.7	2.2	-0.76		0.14		0.06		0.11		0.05		-23.06	5.17
Duanqiao hydrothermal field (DHF), Southwest Indian Ridge	SY117-anemone	*Marianactis sp.*/ muscle	50.4669°E	37.6577°S	1730	NA	164	3.2	2.0	-0.91	0.10	0.30	0.03	0.01	0.03	0.24	0.05	-0.02	0.05	NA	NA
	SY118-2-crab	Munidopsis sp./ muscle	50.4674°E	37.6576°S	1726	5	3899	53.1	1.4	0.04	0.08	0.06	0.04	0.01	0.04	0.00	0.09	0.00	0.04	-18.73	NA
	Replicate									0.00		0.06		0.01		0.04		0.08		NA	NA
	SY118-5-mussel	NA/muscle	50.4674°E	37.6576°S	1726	3	728	3.2	0.60	-0.54	0.27	0.05	0.04	-0.01	0.08	0.00	0.13	0.01	0.18	-32.07	NA
	Replicate									-0.50		0.03		-0.02		-0.02		0.03		NA	NA
	SY118-crab	Munidopsis sp./ muscle	50.4674°E	37.6576°S	1726	NA	606	16.0	2.3	0.52	0.05	0.05	0.06	-0.01	0.01	0.04	0.06	0.00	0.01	-16.55	6.84
	SY118-gastropod	*Chrysomallon squamiferum*/ muscle	50.4674°E	37.6576°S	1726	1	7045	606	8.6	0.30	0.00	0.10	0.05	0.03	0.07	0.08	0.10	0.04	0.02	-23.47	4.95

Kairei hydrothermal field (KHF), Central Indian Ridge	SY138-shrimp	*R. kairei*/muscle	70.0390°E	25.3205°S	2495	6	9.3	BDL	NA	-0.55		0.07		0.03		0.05		-0.06		-13.63	7.74
	SY138-mussel	*Bathymodiolus marisindicus*/ gill	70.0401°E	25.3205°S	2421	1	307	4.0	1.2	0.21	0.07	0.04	0.04	0.02	0.01	0.04	0.02	0.02	0.08	-31.82	0.39
	SY144-snail	Alviniconcha sp./ muscle	70.0404°E	25.3205°S	2422	1	244	3.4	1.2	-0.48		0.10		0.02		0.06		-0.07		-14.29	4.76
	SY145-white snail	*Phymorhynchus sp.*/ muscle	70.0399°E	25.3204°S	2438	1	9.4	BDL	NA	NA		NA		NA		NA		NA		-19.14	2.00
Site F Cold Seep (SFCS), South China Sea	SFCS-1-1	*B. aduloides*/gill	NA	NA	NA	1	920	56.9	6.2	-0.74		0.08		0.01		-0.02		-0.03		-18.44	10.48
	SFCS-1-2	*B. aduloides*/muscle	NA	NA	NA	1	592	37.1	6.3	-0.73		0.06		0.00		-0.07		-0.03		-18.38	9.84
	SFCS-2-1	*G. platifrons*/gill	NA	NA	NA	1	173	4.4	2.6	-0.42		0.18		0.04		0.10		-0.05		-79.99	1.01
	SFCS-2-2	*G. platifrons*/muscle	NA	NA	NA	1	46.0	4.8	10.5	-0.66	0.07	0.20	0.01	0.02	0.04	0.15	0.02	-0.04	0.12	-78.87	0.53

153 Note: Replicate is for Hg isotope measurement; n: number of individuals per sample; dw, dry weight; NA: not available; BDL: below the detection limit.

154

Supplementary Table 3. Summary of Hg isotope compositions and uncertainties in certified reference materials. The larger 2SD values in bold represent the 2σ analytic uncertainties of samples.

	n	**δ^{202}Hg (‰)**	**2SD (‰)**	**Δ^{199}Hg (‰)**	**2SD (‰)**	**Δ^{200}Hg (‰)**	**2SD (‰)**	**Δ^{201}Hg (‰)**	**2SD (‰)**	**Δ^{204}Hg (‰)**	**2SD (‰)**
NIST SRM-8610	50	-0.54	0.05	-0.02	0.03	0.01	0.03	-0.04	0.05	-0.01	0.06
TORT-3	4	0.09	0.09	0.62	0.04	0.05	0.03	0.49	0.09	-0.08	0.06
DORM-4	7	0.44	0.08	1.68	0.09	0.06	0.03	1.37	0.08	-0.08	0.06
Mean 2SD (biota)			**0.09**		**0.06**		**0.03**		**0.09**		**0.06**
MESS-4	4	-1.78	0.12	-0.01	0.04	0.01	0.06	-0.05	0.07	-0.03	0.05
NIST SRM-2702	4	-0.79	0.08	-0.01	0.02	0.00	0.02	-0.03	0.07	-0.02	0.06
NIST SRM-1944	2	-0.44	0.07	0.00	0.04	0.02	0.01	-0.01	0.02	-0.01	0.06
Mean 2SD (sediment)			**0.09**		**0.03**		**0.03**		**0.05**		**0.06**

n: number of measurement replicates.

References

1. German, C. R.; Ramirez-Llodra, E.; Baker, M. C.; Tyler, P. A.; ChEss Scientific Steering, C., Deep-water chemosynthetic ecosystem research during the census of marine life decade and beyond: a proposed deep-ocean road map. *PLoS One* **2011,** *6*, e23259.
2. Van Dover, C. L.; Humphris, S. E.; Fornari, D.; Cavanaugh, C. M.; Collier, R.; Goffredi, S. K.; Hashimoto, J.; Lilley, M. D.; Reysenbach, A. L.; Shank, T. M., Biogeography and Ecological Setting of Indian Ocean Hydrothermal Vents. *Science* **2001,** *294*, 818-823.
3. Ji, F.; Zhou, H.; Yang, Q.; Gao, H.; Wang, H.; Lilley, M. D., Geochemistry of hydrothermal vent fluids and its implications for subsurface processes at the active Longqi hydrothermal field, Southwest Indian Ridge. *Deep Sea Res. Part I Oceanogr. Res. Pap.* **2017,** *122*, 41-47.
4. Tao, C.; Lin, J.; Guo, S.; Chen, Y. J.; Wu, G.; Han, X.; German, C. R.; Yoerger, D. R.; Zhou, N.; Li, H.; Su, X.; Zhu, J., First active hydrothermal vents on an ultraslow-spreading center: Southwest Indian Ridge. *Geology* **2012,** *40*, 47-50.
5. Yang, W.; Tao, C.; Li, H.; Liang, J.; Liao, S.; Long, J.; Ma, Z.; Wang, L., 230Th/238U dating of hydrothermal sulfides from Duanqiao hydrothermal field, Southwest Indian Ridge. *Mar. Geophys. Res.* **2017,** *38*, 71-83.
6. Kumagai, H.; Nakamura, K.; Toki, T.; Morishita, T.; Okino, K.; Ishibashi, J. i.; Tsunogai, U.; Kawagucci, S.; Gamo, T.; Shibuya, T.; Sawaguchi, T.; Neo, N.; Joshima, M.; Sato, T.; Takai, K., Geological background of the Kairei and Edmond hydrothermal fields along the Central Indian Ridge: Implications of their vent fluids' distinct chemistry. *Geofluids* **2008,** *8*, 239-251.
7. Gallant, R. M.; Von Damm, K. L., Geochemical controls on hydrothermal fluids from the Kairei and Edmond Vent Fields, 23°-25°S, Central Indian Ridge. *Geochemistry, Geophys. Geosystems* **2006,** *7*, Q06018.
8. Fang, Y.; Wei, J.; Lu, H.; Liang, J.; Lu, J. a.; Fu, J.; Cao, J., Chemical and structural characteristics of gas hydrates from the Haima cold seeps in the Qiongdongnan Basin of the South China Sea. *J. Asian Earth Sci.* **2019,** *182*, 103924.
9. Liang, Q.; Hu, Y.; Feng, D.; Peckmann, J.; Chen, L.; Yang, S.; Liang, J.; Tao, J.; Chen, D., Authigenic carbonates from newly discovered active cold seeps on the northwestern slope of the South China Sea: Constraints on fluid sources, formation environments, and seepage dynamics. *Deep Sea Res. Part I Oceanogr. Res. Pap.* **2017,** *124*, 31-41.
10. EPA-7473, Mercury in Solids and Solutions by Thermal Decomposition Amalgamation, and Atomic Absorption Spectrophotometry. *USEPA* **2007**.
11. EPA-1630, Methyl Mercury in Water by Distillation, Aqueous Ethylation, Purge and Trap, and CVAFS. *USEPA* **2001**.
12. Chen, J.; Hintelmann, H.; Dimock, B., Chromatographic pre-concentration of Hg from dilute aqueous solutions for isotopic measurement by MC-ICP-MS. *J. Anal. At. Spectrom.* **2010,** *25*, 1402-1409.
13. Zheng, W.; Gilleaudeau, G. J.; Kah, L. C.; Anbar, A. D., Mercury isotope signatures record photic zone euxinia in the Mesoproterozoic ocean. *Proc. Natl. Acad. Sci. U. S. A.* **2018,** *115*, 10594-10599.
14. EPA-1631, Revision E: Mercury in Water by Oxidation, Purge and Trap, and Cold Vapor Atomic Fluorescence Spectrometry *USEPA* **2002**.
15. Meng, M.; Sun, R. Y.; Liu, H. W.; Yu, B.; Yin, Y. G.; Hu, L. G.; Shi, J. B.; Jiang, G. B., An Integrated Model for Input and Migration of Mercury in Chinese Coastal Sediments. *Environ. Sci. Technol.* **2019,** *53*, 2460-2471.
16. Blum, J. D.; Johnson, M. W., Recent developments in mercury stable isotope analysis. *Rev. Mineral. Geochem.* **2017,** *82*, 733-757.
17. Lee, J. H.; Kwon, S. Y.; Lee, H.; Nam, S.-I.; Kim, J.-H.; Joo, Y. J.; Jang, K.; Kim, H.; Yin, R., Climate-Associated Changes in Mercury Sources in the Arctic Fjord Sediments. *ACS Earth Space Chem.* **2021,** *5*, 2398-2407.
18. Zheng, W.; Xie, Z.; Bergquist, B. A., Mercury Stable Isotopes in Ornithogenic Deposits As Tracers of Historical Cycling of Mercury in Ross Sea, Antarctica. *Environ. Sci. Technol.* **2015,** *49*, 7623-32.
19. Blum, J. D.; Bergquist, B. A., Reporting of variations in the natural isotopic composition of mercury. *Anal. Bioanal. Chem.* **2007,** *388*, 353-359.
20. Yin, R.; Feng, X.; Chen, B.; Zhang, J.; Wang, W.; Li, X., Identifying the sources and processes of mercury in subtropical estuarine and ocean sediments using Hg isotopic composition. *Environ. Sci. Technol.* **2015,** *49*, 1347-55.

21. Brown, G., Jr.; Sleeper, K.; Johnson, M. W.; Blum, J. D.; Cizdziel, J. V., Mercury concentrations, speciation, and isotopic composition in sediment from a cold seep in the northern Gulf of Mexico. *Mar. Pollut. Bull.* **2013,** *77*, 308-14.
22. Zhu, C.; Tao, C.; Yin, R.; Liao, S.; Yang, W.; Liu, J.; Barriga, F. J. A. S., Seawater versus mantle sources of mercury in sulfide-rich seafloor hydrothermal systems, Southwest Indian Ridge. *Geochim. Cosmochim. Acta* **2020,** *281*, 91-101.
23. Kim, J.; Lim, D.; Jeong, D.; Xu, Z.; Kim, H.; Kim, J.; Kim, D., Mercury (Hg) geochemistry of mid-ocean ridge sediments on the Central Indian Ridge: Chemical forms and isotopic composition. *Chem. Geol*. **2022,** *604*, 120942.